Single-trapped-ion vibronic Raman laser

C. Di Fidio and W. Vogel
Arbeitsgruppe Quantenoptik, Fachbereich Physik, Universität Rostock, D-18051 Rostock, Germany

R. L. de Matos Filho and L. Davidovich
Instituto de Física, Universidade Federal do Rio de Janeiro, Caixa Postal 68528, 21945-970 Rio de Janeiro, RJ, Brazil
(Received 23 August 2001; published 13 December 2001)

We propose a model for a single-trapped-ion vibronic Raman laser and study its dynamics by using quantum-trajectory methods. In our treatment, it is essential that both the cavity field of the high-finesse optical cavity and the center-of-mass vibrational motion of the trapped ion be quantized. A transition from a super-Poissonian light source to a Poissonian lasing regime is obtained by increasing the Raman coupling constant. Furthermore, we demonstrate that a nonclassical regime can be realized, where the photon statistics becomes sub-Poissonian and the photons leak out of the cavity in an antibunched manner. This is achieved by exploiting nonlinear Stark shifts inherent in the model, which depend on both the number of cavity photons and the number of vibrational quanta.

DOI: 10.1103/PhysRevA.65.013811 PACS number(s): 42.50.Ct, 32.80.−t, 42.55.−f, 42.50.Vk

I. INTRODUCTION

The possibility to obtain a laser operating with a single atom as the active medium recently became feasible, thanks to developments in experimental quantum optics. There have been several theoretical contributions on one-atom lasers in the past decade [1–4]. An analysis showing that laser action is possible with one atom was performed in Ref. [1]. In Refs. [2,3], the spectral properties of a single two-level atom interacting with one lasing mode have been studied. Moreover, a single-atom laser consisting of a three-level system has also been discussed [4]. In the microwave domain, maser action with a very small mean number of atoms was already demonstrated in the micromaser [5,6] some years ago. More recently, a microlaser [7] has been realized in which a weak beam of excited atoms traverses an optical cavity.

Nowadays it is possible, instead of using weak atom beams as the active medium, to trap single atoms in a cavity. Recent experiments have successfully realized the trapping of a single cold atom in a high-finesse optical cavity [8–10]. In these cases, the atoms are trapped by the radiation field. Alternatively one may also combine a quadrupole trap to localize a single trapped ion in a high-Q optical cavity, which would allow one to control the trapping conditions and the atom-field interaction independently of each other.

The first analysis of an experimental realization of a trapped-ion laser has been given by Meyer *et al.* [11,12]. The authors have shown that the operational regime of a single-trapped-ion laser, in contrast to conventional lasers, can have two thresholds, namely self-quenching effects and lasing without inversion. Effects of quantized center-of-mass motion on the action of a single-trapped-ion laser have also been analyzed [13,14]. In Ref. [13], the inversion required for the lasing is realized, in analogy to standard laser models, by using an electronic three-level scheme. In this case, the quantized motion modifies the laser action to some extent, but it is not necessary for realizing the lasing itself. In Ref. [14], the inversion rests upon the existence of vibronic transitions, so that the quantization of the ion's motion is of crucial importance for the lasing phenomenon. The latter system, however, is difficult to realize, since the inversion in the considered model occurs on the second vibronic sideband. Since the Lamb-Dicke regime is considered, the coupling to a quantized cavity field on the second sideband is very weak so that lasing is difficult to achieve.

The aim of our paper is to propose a single-trapped-ion Raman laser that differs from previous models in the following respects. First, the laser action requires the quantized motion and the inversion is obtained already on the first vibronic sideband. Second, the Lamb-Dicke regime is not necessary to obtain laser action. The first point is important to produce a sufficiently strong coupling between the inverted atomic transitions and the quantized cavity field mode, which is realized by Raman coupling. The second point may be used to increase the atom-field coupling strength. Moreover, it is known that the atom-radiation interaction outside the Lamb-Dicke regime may display significant nonlinear effects [15,16], which can be of interest here to modify the quantum statistical properties of the laser field. In particular, we will see that nonlinear Stark-shift effects can be controlled in order to produce a nonclassical laser source emitting sub-Poissonian and antibunched radiation. The atomic energy-level scheme under study is close to the situation in experiments with a single $^9Be^+$ ion [17,18], which might be used to implement the laser model under consideration.

The paper is organized as follows. In Sec. II, we introduce our model for the single-trapped-ion Raman laser and we derive the master equation for the system under study. In Sec. III, we present the basic ideas for solving the master equation by using quantum-trajectory methods. In Sec. IV, we demonstrate that, depending on the strength of the atom-field coupling, the radiation inside and outside the laser cavity undergoes a transition from a super-Poissonian, bunched light field to a Poissonian laser regime, with only about three photons inside the cavity. In particular, we focus our attention on the electronic-state inversion, the photon-number probability distribution of the intracavity field, the photon-number probability distribution of the photons detected out-

side the cavity, and the second-order intensity correlation function. In Sec. V, we show how a nonclassical regime can be obtained by appropriate control of Stark shifts that depend on both the motional quantum state and on the state of the cavity mode. Clear signatures of sub-Poissonian photon statistics and photon antibunching are observed. In Sec. VI, we present a summary and some conclusions.

II. MODEL AND BASIC EQUATIONS

Let us consider a trapped ion placed inside a high-finesse optical cavity. The scheme under consideration is shown in Fig. 1. We denote by ν the secular frequency of the RF-Paul trap along the x direction, coinciding with the axis of the optical cavity. In our configuration, a laser beam of frequency ω_1 and the cavity mode of frequency ω_C provide a Raman coupling between the electronic levels $|1\rangle$ and $|2\rangle$, being detuned by Δ from the intermediate electronic level $|4\rangle$. In this way, the vibrational quantum state of the center-of-mass motion of the trapped ion is coupled to the field of the cavity mode. We also introduce an adjustable frequency shift $\delta\omega_1$ for the first laser. A second laser of frequency ω_2, tuned to the first red sideband, couples directly levels $|1\rangle$ and $|3\rangle$. Moreover, an incoherent field of frequency $\omega_{\rm inc}$ is resonant with the transition $|1\rangle\leftrightarrow|2\rangle$. The properties of the partially transmitting mirror are described by the parameter κ, the cavity photon escape rate. The relaxation rates from level $|3\rangle$ to levels $|1\rangle$ and $|2\rangle$ are γ and γ', respectively.

The master equation for the trapped ion under the influence of the laser fields and the cavity mode is given by

$$\frac{\partial\hat{\varrho}}{\partial t}=\frac{1}{i\hbar}[\hat{H}(t),\hat{\varrho}]-\frac{\gamma+\gamma'}{2}(\hat{A}_{33}\hat{\varrho}+\hat{\varrho}\hat{A}_{33})+\gamma\int_{-1}^{1}dq\,w(q)\hat{A}_{13}e^{iqk_{31}\hat{x}}\hat{\varrho}\,e^{-iqk_{31}\hat{x}}\hat{A}_{31}+\gamma'\int_{-1}^{1}dq\,w(q)\hat{A}_{23}e^{iqk_{32}\hat{x}}\hat{\varrho}\,e^{-iqk_{32}\hat{x}}\hat{A}_{32}+\frac{\kappa}{2}(-\hat{b}^{\dagger}\hat{b}\hat{\varrho}-\hat{\varrho}\hat{b}^{\dagger}\hat{b}+2\hat{b}\hat{\varrho}\hat{b}^{\dagger}). \tag{1}$$

Here $\hat{\varrho}(t)$ is the density operator that describes the electronic degree of freedom $|i\rangle$ $(i=1,\ldots,4)$, the motion of the center of mass of the ion in the x direction, and the quantum state of the cavity-mode field. Moreover, $k_{31}=\omega_{31}/c$, $k_{32}=\omega_{32}/c$, and $w(q)=\frac{3}{8}(1+q^2)$ is the angular distribution of the spontaneously emitted radiation. The terms in Eq. (1) containing γ and γ' describe recoil effects of the spontaneously emitted photon of modulo wave vector k_{31} and k_{32}, respectively. The last term in Eq. (1) describes the cavity losses, where $\hat{b}$ and $\hat{b}^{\dagger}$ are the annihilation and creation operators of a photon in the cavity mode. The Hamiltonian $\hat{H}(t)=\hat{H}_0+\hat{H}_I(t)$ is composed of the free Hamiltonian

$$\hat{H}_0=\hbar\nu\hat{a}^{\dagger}\hat{a}+\hbar\omega_C\hat{b}^{\dagger}\hat{b}+\sum_{i=1}^{4}\hbar\omega_i\hat{A}_{ii}, \tag{2}$$

where $\hat{a}$ and $\hat{a}^{\dagger}$ are the annihilation and creation operators of quanta of vibrational motion, and the interaction Hamiltonian of the atom with the lasers and the cavity field,

$$\frac{\hat{H}_I(t)}{\hbar}=\Omega_{\rm inc}(t)e^{i(k_{\rm inc}\hat{x}-\omega_{\rm inc}t)}\hat{A}_{21}+\Omega_1 e^{i[k_1\hat{x}-(\omega_1+\delta\omega_1)t]}\hat{A}_{42}+\Omega_2 e^{i(k_2\hat{x}-\omega_2 t)}\hat{A}_{31}+g\cos(k_C\hat{x}+\varphi_C)\hat{b}\hat{A}_{41}+\text{H.c.} \tag{3}$$

Here Ω_1, Ω_2, and $\Omega_{\rm inc}$ are the Rabi frequencies of the first, second, and incoherent laser, respectively. Moreover, g is the coupling strength between the cavity mode and the $|1\rangle\leftrightarrow|4\rangle$ transition. The phase φ_C describes the position of the harmonic trap with respect to the cavity standing wave. Moreover, $\hat{A}_{ij}=|i\rangle\langle j|$ $(i,j=1,\ldots,4)$ are flip operators for electronic transitions $|j\rangle\rightarrow|i\rangle$, and the amplitude of the incoherent laser is given by

$$\Omega_{\rm inc}(t)=\Omega_{\rm inc}e^{i\varphi(t)}, \tag{4}$$

where $\varphi(t)$ is a stochastic phase.

In this scheme, a population inversion is obtained by combining a cooling mechanism with a resonant incoherent laser drive. The second laser together with the spontaneous emissions γ,γ' produce the cooling mechanism for the motional state of the ion. The incoherent laser is used to destroy coherence between levels $|1\rangle$ and $|2\rangle$ and it saturates the transition $|1\rangle\leftrightarrow|2\rangle$. We will show that the cooling to the motional ground state together with the saturation provides the desired population inversion on the first vibrational sideband, that is, the $|2,k\rangle\leftrightarrow|1,k+1\rangle$ transitions, where $k=0,\ldots,\infty$ labels the vibrational states.

In order to eliminate fast oscillating terms in the dynamics described by the Hamiltonian given in Eq. (3), it is conve-

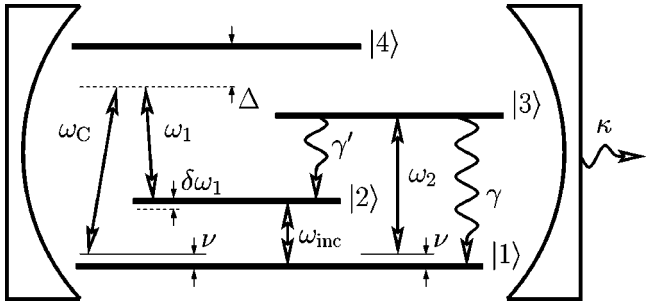

FIG. 1. Scheme for the vibronic laser. A trapped ion is placed inside a high-finesse optical cavity. The first laser of frequency ω_1 and the cavity mode of frequency ω_C provide a Raman coupling between the electronic levels $|1\rangle$ and $|2\rangle$, here detuned by Δ from the intermediate level $|4\rangle$. The frequency difference $\omega_C-\omega_1$ is tuned close to $\omega_{21}-\nu$, where $\delta\omega_1$ is an adjustable frequency shift for the first laser. A second laser of frequency ω_2 is tuned to the first red sideband relative to the transition $|1\rangle\leftrightarrow|3\rangle$. The dipole relaxation rates from level $|3\rangle$ to level $|1\rangle$ and $|2\rangle$ are γ and γ', respectively, and κ is the photon escape rate of the cavity. An incoherent field of frequency $\omega_{\rm inc}$ is resonant to the transition $|1\rangle\leftrightarrow|2\rangle$.

nient to change into the interaction picture with respect to $\hat{H}_0-\hbar\Delta\hat{A}_{44}$. This yields the following interaction Hamiltonian:

$$\frac{\hat{H}_{\rm int}(t)}{\hbar}=\{\Omega_{\rm inc}(t)e^{ik_{\rm inc}\hat{x}(t)}\hat{A}_{21}+\Omega_1 e^{i[k_1\hat{x}(t)-\delta\omega_1 t]}\hat{A}_{42}+\Omega_2 e^{i[k_2\hat{x}(t)+\nu t]}\hat{A}_{31}+g\cos[k_C\hat{x}(t)+\varphi_C]\times e^{i\nu t}\hat{b}\hat{A}_{41}+\text{H.c.}\}+\Delta\hat{A}_{44}, \tag{5}$$

where now the $\hat{x}$ operator is time-dependent

$$\hat{x}(t)=\sqrt{\frac{\hbar}{2M\nu}}(\hat{a}e^{-i\nu t}+\hat{a}^\dagger e^{i\nu t}), \tag{6}$$

with M being the mass of the ion. From Eq. (1) we calculate the differential equations for the electronic density-matrix elements $\langle i|\hat{\varrho}|j\rangle$ and insert the adiabatically solved off-diagonal elements, due to the far-detuned situation, into the equations for the other elements. In the weak driving-field limit it is possible to obtain an equation describing the evolution of the electronic $|1\rangle\leftrightarrow|2\rangle$ transition together with the quantized vibrational center-of-mass motion and the cavity field. Similar to the derivations in [19], we keep only the leading terms in the Rabi frequencies and we adiabatically eliminate $\hat{\varrho}_{33}$ and $\hat{\varrho}_{44}$. In this way, it is possible to obtain the following master equation for the density operator $\hat{\rho}$ that describes the electronic degrees of freedom $|1\rangle$ and $|2\rangle$, the motional subsystem, and the cavity field:

$$\frac{\partial\hat{\rho}}{\partial t}=\frac{1}{i\hbar}[\hat{H}'\hat{\rho}-\hat{\rho}\hat{H}'^{\dagger}]+\int_{-1}^{1}dq\,\hat{J}_q^{(1)}(t)\hat{\rho}\hat{J}_q^{(1)\dagger}(t)+\int_{-1}^{1}dq\,\hat{J}_q^{(2)}(t)\hat{\rho}\hat{J}_q^{(2)\dagger}(t)+\hat{J}_C\hat{\rho}\hat{J}_C^{\dagger}. \tag{7}$$

The non-Hermitian Hamiltonian $\hat{H}'$ reads

$$\frac{\hat{H}'}{\hbar}=\frac{\hat{H}_{\rm eff}}{\hbar}+[\Omega_{\rm inc}(t)\hat{f}_0(\hat{a}^\dagger\hat{a};\eta_{\rm inc})\hat{A}_{21}+\text{H.c.}]-\frac{i}{2}\left\{\frac{4|\Omega_2|^2}{(\gamma+\gamma')}\eta_2^2\hat{a}^\dagger g[\hat{f}_1(\hat{a}^\dagger\hat{a};\eta_2)]^2\hat{a}\hat{A}_{11}+\kappa\hat{b}^\dagger\hat{b}\right\}, \tag{8}$$

where the operator functions $\hat{f}_m$ are given by

$$\hat{f}_m(\hat{a}^\dagger\hat{a};\eta)=\sum_{n=0}^{\infty}|n\rangle\langle n|\frac{n!}{(n+m)!}L_n^{(m)}(\eta^2)e^{-\eta^2/2}, \tag{9}$$

with $L_n^{(m)}(x)$ being generalized Laguerre polynomials. In order to write Eq. (8), we have eliminated fast-oscillating terms in the interaction with the incoherent laser and the second laser, see Appendix A. Here $\eta_{\rm inc}$ and η_2 are the Lamb-Dicke parameters related to $k_{\rm inc}$ and to k_2, respectively ($\eta_2=\sqrt{\hbar k_2^2/2M\nu}$). Moreover, the effective Hamiltonian $\hat{H}_{\rm eff}$ is expressed by

$$\hat{H}_{\rm eff}=\hat{H}_{\rm eff}^R+\hat{H}_{\rm eff}^S, \tag{10}$$

where the Raman Hamiltonian $\hat{H}_{\rm eff}^R$ and the Stark-shift term $\hat{H}_{\rm eff}^S$ are given, before elimination of fast-oscillating terms, by

$$\frac{\hat{H}_{\rm eff}^R(t)}{\hbar}=-\Omega_R\cos(k_C\hat{x}(t)+\varphi_C)e^{i[k_1\hat{x}(t)-(\delta\omega_1+\nu)t]}\times\hat{b}^\dagger\hat{A}_{12}+\text{H.c.}, \tag{11}$$

where

$$\Omega_R=\frac{g^*\Omega_1}{\Delta} \tag{12}$$

is the Raman coupling constant, and

$$\frac{\hat{H}_{\rm eff}^S(t)}{\hbar}=-\frac{|g|^2}{\Delta}[\cos(k_C\hat{x}(t)+\varphi_C)]^2\hat{b}^\dagger\hat{b}\hat{A}_{11}-\frac{|\Omega_1|^2}{\Delta}\hat{A}_{22}. \tag{13}$$

The three different jump operators in Eq. (7) are defined by

$$\hat{J}_q^{(1)}(t)=\sqrt{\frac{4\gamma w(q)}{(\gamma+\gamma')^2}}\Omega_2 e^{iqk_{31}\hat{x}(t)}\hat{f}_1(\hat{a}^\dagger\hat{a};\eta_2)(\eta_2\hat{a})\hat{A}_{11}, \tag{14}$$

$$\hat{J}_q^{(2)}(t)=\sqrt{\frac{4\gamma' w(q)}{(\gamma+\gamma')^2}}\Omega_2 e^{iqk_{32}\hat{x}(t)}\hat{f}_1(\hat{a}^\dagger\hat{a};\eta_2)(\eta_2\hat{a})\hat{A}_{21}, \tag{15}$$

$$\hat{J}_C=\sqrt{\kappa}\hat{b}. \tag{16}$$

The jump operators $\hat{J}_q^{(1)}$ and $\hat{J}_q^{(2)}$ describe the cooling effects due to electronic transitions $|1\rangle\rightarrow|1\rangle$ and $|1\rangle\rightarrow|2\rangle$, respectively (the transitions include the level $|3\rangle$, which was adiabatically eliminated, and therefore does not appear explicitly). The jump operator $\hat{J}_C$ describes a photon emission from the cavity, i.e., the annihilation of a photon in the cavity mode. Moreover, the stochastic phase related to the amplitude of the incoherent laser, see Eq. (4), satisfies the equation

$$\varphi(t+dt)=\varphi(t)+\sqrt{2\Gamma_{\rm inc}}\,dW, \tag{17}$$

where $\Gamma_{\rm inc}$ is the linewidth of the laser and dW is the increment of the corresponding Wiener process.

After elimination of fast-oscillating terms, see Appendix A, Eq. (13) transforms into

$$\frac{\hat{H}^S_{\rm eff}}{\hbar} = -\frac{|g|^2}{2\Delta}[1+\cos(2\varphi_C)\hat{f}_0(\hat{a}^\dagger\hat{a};\eta_{2C})] \times \hat{b}^\dagger\hat{b}\hat{A}_{11} - \frac{|\Omega_1|^2}{\Delta}\hat{A}_{22}, \tag{18}$$

where η_{2C} is the Lamb-Dicke parameter related to $2k_C$. Moreover, if we choose $\delta\omega_1=0$, Eq. (11) becomes, under the same approximation, see Appendix A,

$$\frac{\hat{H}^R_{\rm eff}}{\hbar} = -\frac{1}{2}\Omega_R e^{i\varphi_C}(i\eta_+\hat{a}^\dagger)\hat{f}_1(\hat{a}^\dagger\hat{a};\eta_+)\hat{b}^\dagger\hat{A}_{12} + \text{H.c.}, \tag{19}$$

where η_+ is the Lamb-Dicke parameter related to (k_1+k_C) and we have neglected the terms with η_-, the Lamb-Dicke parameter related to (k_1-k_C), since $\eta_- \ll 1$. It is also often useful to neglect the constant Stark-shift term $-\hbar(|\Omega_1|^2/\Delta)\hat{A}_{22}$ in Eq. (18). This can be done as described in Appendix A. In this way we obtain the following expression for $\hat{H}^S_{\rm eff}$:

$$\frac{\hat{H}^S_{\rm eff}}{\hbar} = -\frac{|g|^2}{2\Delta}[1+\cos(2\varphi_C)\hat{f}_0(\hat{a}^\dagger\hat{a};\eta_{2C})]\hat{b}^\dagger\hat{b}\hat{A}_{11}. \tag{20}$$

III. QUANTUM-TRAJECTORY SIMULATIONS

A direct solution of Eq. (7) is not an easy analytical task. This is why we are led to use numerical methods in order to solve this equation. Using Eqs. (14)–(16), it is easy to see that

$$\int_{-1}^{1} dq\,\hat{J}_q^{(1)\dagger}(t)\hat{J}_q^{(1)}(t) = \frac{4\gamma|\Omega_2|^2}{(\gamma+\gamma')^2}\eta_2^2\hat{a}^\dagger[\hat{f}_1(\hat{a}^\dagger\hat{a};\eta_2)]^2\hat{a}\hat{A}_{11}, \tag{21}$$

$$\int_{-1}^{1} dq\,\hat{J}_q^{(2)\dagger}(t)\hat{J}_q^{(2)}(t) = \frac{4\gamma'|\Omega_2|^2}{(\gamma+\gamma')^2}\eta_2^2\hat{a}^\dagger[\hat{f}_1(\hat{a}^\dagger\hat{a};\eta_2)]^2\hat{a}\hat{A}_{11}, \tag{22}$$

$$\hat{J}_C^\dagger\hat{J}_C = \kappa\hat{b}^\dagger\hat{b}. \tag{23}$$

This shows that Eq. (7) is in the so-called Lindblad form, so that it can be solved by quantum-trajectory methods [20–24].

In order to perform our quantum-trajectory simulations, we proceed as follows. We start with the ion in its motional and electronic ground state, and with no photon inside the cavity field, so that the initial quantum state $|\psi(0)\rangle = |1,0,0\rangle$, where the first index in the ket corresponds to the electronic state, the second to the motional state, and the third to the cavity field, respectively. For each trajectory we start from the initial state $|\psi(0)\rangle$ and then we integrate the Schrödinger equation

$$i\hbar\frac{\partial|\psi\rangle}{\partial t} = \hat{H}'|\psi\rangle. \tag{24}$$

Because $\hat{H}'$ is non-Hermitian, the norm $\||\psi(t)\rangle\|^2$ is not constant, and it is actually decaying from its initial value equal to 1. To determine the time when a jump occurs, we proceed as follows [21]. A jump occurs when $1-\||\psi(t)\rangle\|^2=\epsilon$, with $\epsilon\in[0,1]$ being a random number drawn from a uniform distribution. To determine which one of the three jumps occurs, we make use of the relative probabilities Π_1, Π_2, and Π_3 for jump one, two, and three to occur, respectively, given by

$$\Pi_1 = \frac{1}{\Pi}\langle\psi(t)|\int_{-1}^{1} dq\,\hat{J}_q^{(1)\dagger}(t)\hat{J}_q^{(1)}(t)|\psi(t)\rangle, \tag{25}$$

$$\Pi_2 = \frac{1}{\Pi}\langle\psi(t)|\int_{-1}^{1} dq\,\hat{J}_q^{(2)\dagger}(t)\hat{J}_q^{(2)}(t)|\psi(t)\rangle, \tag{26}$$

$$\Pi_3 = \frac{1}{\Pi}\langle\psi(t)|\hat{J}_C^\dagger\hat{J}_C|\psi(t)\rangle, \tag{27}$$

where

$$\Pi = \langle\psi(t)|\int_{-1}^{1} dq[\hat{J}_q^{(1)\dagger}\hat{J}_q^{(1)} + \hat{J}_q^{(2)\dagger}\hat{J}_q^{(2)}] + \hat{J}_C^\dagger\hat{J}_C|\psi(t)\rangle. \tag{28}$$

Writing $|\psi(t)\rangle = |1\rangle|\psi_1(t)\rangle + |2\rangle|\psi_2(t)\rangle$, where now $|\psi_1(t)\rangle$ and $|\psi_2(t)\rangle$ refer to the vibrational and cavity modes, and using Eqs. (21)–(23), we can write these probabilities as

$$\Pi_1 = \frac{1}{\Pi}\frac{4\gamma|\Omega_2|^2}{(\gamma+\gamma')^2}\eta_2^2\langle\psi_1(t)|\hat{a}^\dagger[\hat{f}_1(\hat{a}^\dagger\hat{a};\eta_2)]^2\hat{a}|\psi_1(t)\rangle, \tag{29}$$

$$\Pi_2 = \frac{1}{\Pi}\frac{4\gamma'|\Omega_2|^2}{(\gamma+\gamma')^2}\eta_2^2\langle\psi_1(t)|\hat{a}^\dagger[\hat{f}_1(\hat{a}^\dagger\hat{a};\eta_2)]^2\hat{a}|\psi_1(t)\rangle, \tag{30}$$

$$\Pi_3 = \frac{\kappa}{\Pi}\langle\psi(t)|\hat{b}^\dagger\hat{b}|\psi(t)\rangle, \tag{31}$$

where

$$\Pi = \frac{4\eta_2^2|\Omega_2|^2}{(\gamma+\gamma')}\langle\psi_1(t)|\hat{a}^\dagger[\hat{f}_1(\hat{a}^\dagger\hat{a};\eta_2)]^2\hat{a}|\psi_1(t)\rangle + \kappa\langle\psi(t)|\hat{b}^\dagger\hat{b}|\psi(t)\rangle. \tag{32}$$

If a jump one, Eq. (14), or a jump two, Eq. (15), occurs, we have to use a new random number $q\in[-1,1]$ drawn from the distribution given by $w(q)=\frac{3}{8}(1+q^2)$. After the action of a jump operator, the state is renormalized and the next jump is determined again as described above. We repeat this procedure for N trajectories. The density matrix at a time t is obtained by averaging over all realizations

$$\hat{\rho}(t) = \frac{1}{N}\sum_{i=1}^{N}|\tilde{\psi}^{(i)}(t)\rangle\langle\tilde{\psi}^{(i)}(t)|, \tag{33}$$

with $|\tilde{\psi}^{(i)}(t)\rangle = |\psi^{(i)}(t)\rangle/\||\psi^{(i)}(t)\rangle\|$.

IV. LASING REGIME

In this section, we are going to demonstrate that, under chosen conditions, the system considered here allows one to approach a lasing regime. We will first demonstrate that population inversion is obtained even in the presence of the losses inherent to the system, including the cavity loss and spontaneous emission. The quantum-trajectory simulations render it possible to study the statistics of both the intracavity field and the external field as well as the intensity correlation behavior of the external field. It will be shown that a mean number of cavity photons between two and three is sufficient to obtain typical signatures of a transition from a super-Poissonian, bunched light source to a Poissonian lasing regime.

In the simulations we have chosen the following parameters. For the Lamb-Dicke parameters $\eta_+ = \eta_{2C} = 0.2$, $\eta_{inc} = 0.001$, $\eta_2 = 0.14$. Moreover, $\Omega_{inc} = \Gamma_{inc} = 1$ MHz, $\kappa = 0.1$ MHz, $\Delta = 600$ MHz, $\nu = 100$ MHz, $\Omega_2 = 10$ MHz, and $\gamma = \gamma' = 5$ MHz. The parameter Ω_1 was chosen equal to g and its range was tested from a value of $\Omega_1 = g = 40$ MHz to a value of $\Omega_1 = g = 60$ MHz. This corresponds to varying the Raman coupling Ω_R from a value $\Omega_R = 2.66$ MHz to a value $\Omega_R = 6.0$ MHz. Note that the condition $\Omega_2, \gamma \ll \nu$ is satisfied, so that we have a resolved sideband. Moreover, $\eta_2 \Omega_2 \ll (\gamma + \gamma')$ and $\Omega_1, g \ll \Delta$ so that the adiabatic elimination of the levels $|3\rangle$ and $|4\rangle$ can be done.

It is also important to carefully consider the Stark-shift term in Eq. (20), which depends on both the number of photons and the motional excitation. In the Lamb-Dicke limit, where $\hat{f}_0(\hat{a}^\dagger \hat{a}; \eta_{2C}) \to 1$, the contribution of the Stark shift disappears if we choose for the phase of the cavity the value $\varphi_C = \pi/2$. In this section we will choose $\varphi_C = \pi/2$, even if we have $\eta_{2C} = 0.2$. This allows us to minimize the effects of the motion- and field-dependent Stark shift. We get then

$$\frac{\hat{H}_{\text{eff}}}{\hbar} = \left[\frac{1}{2} \Omega_R \eta_+ \hat{a}^\dagger \hat{f}_1(\hat{a}^\dagger \hat{a}; \eta_+) \hat{b}^\dagger \hat{A}_{12} + \text{H.c.} \right] - \frac{|g|^2}{2\Delta} [1 - \hat{f}_0(\hat{a}^\dagger \hat{a}; \eta_{2C})] \hat{b}^\dagger \hat{b} \hat{A}_{11}, \tag{34}$$

and the dynamics of the system is considerably simplified. The consequences of more dominant Stark shifts will be studied in Sec. V.

The density matrix $\hat{\rho}(t)$ used in the present section is obtained as discussed in Sec. III, i.e., from Eq. (33). It can be expressed in the basis of atomic and photon states using the notation

$$\hat{\rho}(t) = \sum_{i,j=0}^{2} \sum_{k,l=0}^{\infty} \sum_{m,n=0}^{\infty} \rho_{i,k;j,l}^{m;n} |i,k,m\rangle\langle j,l,n|, \tag{35}$$

where $|i\rangle$, $|j\rangle$ are the electronic levels, $|k\rangle$, $|l\rangle$ are number states for the vibrational motion, and $|m\rangle$, $|n\rangle$ denote number states for the cavity mode.

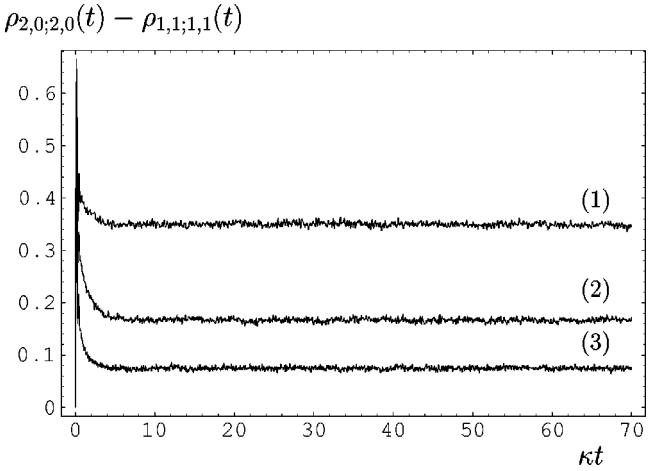

FIG. 2. Electronic-state inversion $\rho_{2,0;2,0}(t) - \rho_{1,1;1,1}(t)$. The figures are obtained for different values of the parameter $\Omega_1 = g$: 40 MHz (1), 50 MHz (2), and 60 MHz (3). The ensemble average is performed over 5000 trajectories.

A. Electronic-state inversion

Photon emission into the cavity mode is obtained via the Raman coupling. This is described by the term $\hat{a}^\dagger \hat{f}_1(\hat{a}^\dagger \hat{a}; \eta_+) \hat{b}^\dagger \hat{A}_{12}$ in $\hat{H}_{\text{eff}}$, see Eq. (34). The electronic transition $|2\rangle \to |1\rangle$ is accompanied by the creation of both a photon in the cavity mode and a quantum of vibrational motion. Of course, there is also a competing mechanism that tends to subtract photons from the cavity, formally the Hermitian conjugate in Eq. (34), i.e., the term $\hat{f}_1(\hat{a}^\dagger \hat{a}; \eta_+) \hat{a} \hat{b} \hat{A}_{21}$. Photon emission dominates over absorption if there is a vibronic population inversion, that is,

$$\rho_{2,k;2,k} > \rho_{1,k+1;1,k+1}, \quad k = 0, \ldots, \infty, \tag{36}$$

with

$$\rho_{i,k;i,k}(t) = \sum_{m=0}^{\infty} \rho_{i,k;i,k}^{m;m}. \tag{37}$$

The cooling to the motional ground state together with the saturation due to the incoherent laser provides the desired population inversion on the first vibrational sideband, that is, the $|2,k\rangle \leftrightarrow |1,k+1\rangle$ transitions. In Fig. 2, the population inversion is shown for $k = 0$. Due to the cooling mechanism this is the dominant transition, but also for $k > 0$ a population inversion is obtained in the simulations.

B. Intracavity field

The average number of photons inside the cavity is obtained from $\hat{\rho}(t)$ via

$$\langle \hat{b}^\dagger \hat{b} \rangle_t = \text{Tr}[\hat{b}^\dagger \hat{b} \hat{\rho}(t)]. \tag{38}$$

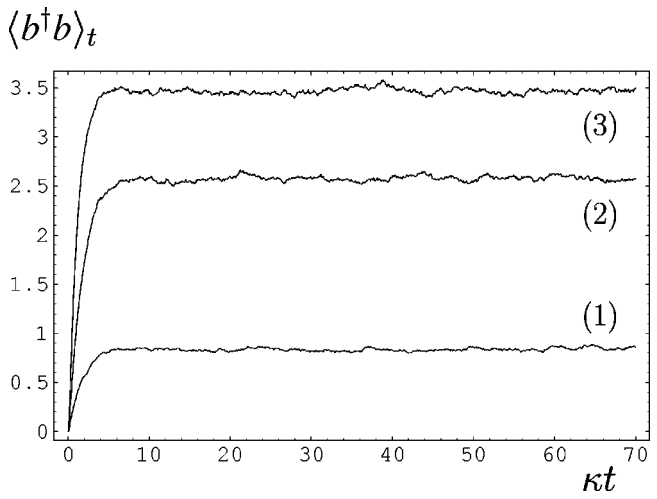

FIG. 3. Average number of photons inside the cavity, for different values of the parameter $\Omega_1 = g$: 40 MHz (1), 50 MHz (2), and 60 MHz (3). The ensemble average is performed over 5000 trajectories.

As shown in Fig. 3, after a transient regime, which is practically concluded after less than ten cavity decay times, a stationary regime is reached. As the Raman coupling constant Ω_R, see Eq. (12), increases from a value of 2.66 MHz to a value of 6.0 MHz, the average number of photons inside the cavity goes from a value of approximately 0.8 to a value of approximately 3.5.

In order to characterize the intracavity field, the mean number of cavity photons is of course not sufficient. It is useful to consider the photon-number probability distribution P_n. This is obtained from $\hat{\rho}(t)$ by

$$P_n = \mathrm{Tr}[|n\rangle\langle n|\hat{\rho}(t)]. \tag{39}$$

This distribution is shown, for different values of the Raman coupling constant, in Fig. 4. From it one can calculate the expression for the relative variance of the photon number statistics, $\overline{(\Delta n)^2}/\overline{n}$, where $\overline{(\cdots)} = \Sigma_n \cdots P_n$. As is well known, for a Poissonian distribution $\overline{(\Delta n)^2}/\overline{n} = 1$. In our case, P_n is changed from a super-Poissonian distribution to a Poissonian distribution by increasing the Raman coupling constant.

C. External field

Let us consider a detector situated outside the cavity. For a detector of unit efficiency every emission of a photon from the cavity produces a photoelectric count or a ''click'' in the detector. To characterize the field emitted from the cavity, one has to analyze the statistics of the photoelectric counts. The photon-number probability distribution $P_n(t,T)$ is obtained by considering a given time interval T (integration time), and by looking at how many clicks are recorded in the time interval $[t, t+T)$. The number of clicks registered in a given time interval is not constant and its value is a number that is distributed around an average value. This average value increases with the size of the time interval. For the

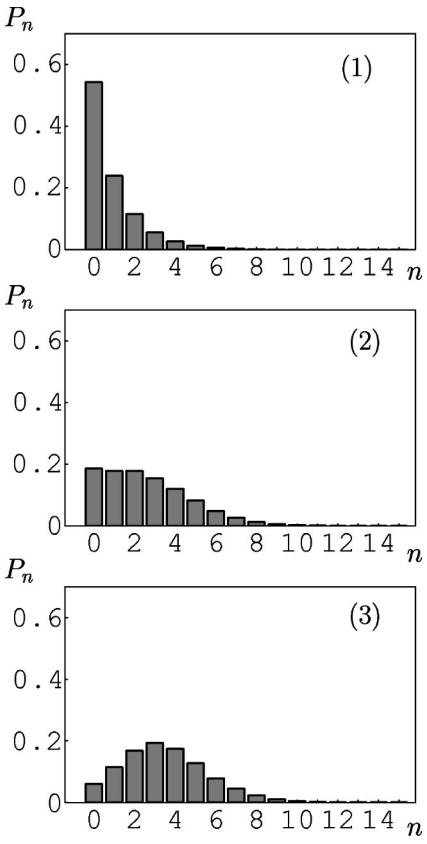

FIG. 4. Photon-number probability distribution for the photons inside the cavity at the time $t = 70/\kappa$. The figures are for different values of the parameter $\Omega_1 = g$: 40 MHz (1), 50 MHz (2), and 60 MHz (3). The values for $\overline{(\Delta n)^2}/\overline{n}$ are 1.84 (1), 1.73 (2), and 1.26 (3). The ensemble average is performed over 5000 trajectories.

simple case of a coherent light source of constant intensity $\overline{I}$, it is known that $P_n(T)$ is given by a Poissonian distribution

$$P_n(T) = \frac{\overline{n}^n}{n!}\exp(-\overline{n}), \tag{40}$$

where $\overline{n}$ is proportional to $\overline{I}T$.

To obtain the distribution $P_n(T)$ we have proceeded as follows. We have chosen a time interval T in the stationary regime region, i.e., for $t > 10/\kappa$, and we have counted for each trajectory how many clicks were registered in $[t, t+T)$. In our case, this is equivalent to the number of cavity jumps occurring in this time interval. This number differs, in general, from one trajectory to the other. Repeating this procedure for a large number of trajectories, a probability distribution is obtained. The photon-number probability distributions are shown, for different values of the Raman coupling constant, in Fig. 5, where the integrating time was chosen $T = 1/\kappa$. From these distributions we can obtain the relative variance of the click number statistics. A transition from a super-Poissonian light source to a coherent one is observed.

Let us compare the photon number distributions inside and outside the cavity as given in Fig. 4 and Fig. 5, respec-

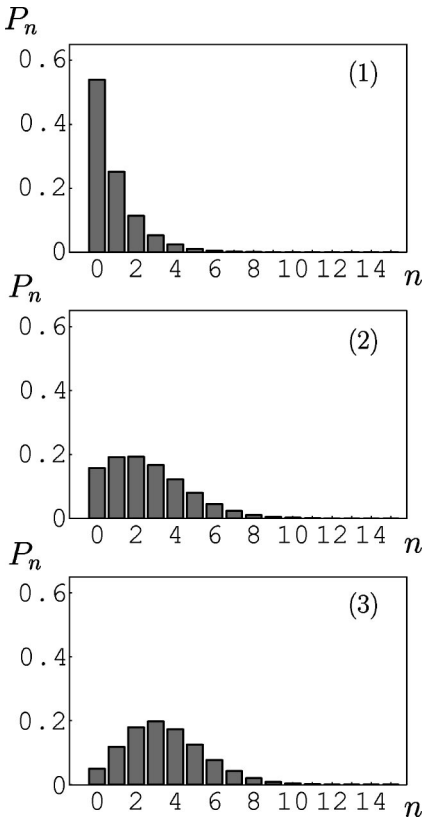

FIG. 5. Photon-number probability distribution for the photons detected outside the cavity for an integration time $T=1/\kappa$. The figures are for different values of the parameter $\Omega_1=g$: 40 MHz (1), 50 MHz (2), and 60 MHz (3). The values for $\overline{(\Delta n)^2}/\overline{n}$ are 1.74 (1), 1.58 (2), and 1.19 (3). The ensemble average is performed over 5000 trajectories.

tively. It is obvious that the relative noise, $\overline{(\Delta n)^2}/\overline{n}$, in the output field is less than in the intracavity field. To understand this fact, we remind the reader of the basic principles of photocounting theory; for details, see, e.g., [25]. In particular, for recording the statistics of photoelectric counts of a traveling light field, one needs to choose a measurement-time interval T over which the events are counted. By increasing the size of this interval, the statistics becomes more and more Poissonian. In our case, the chosen interval size of $T=1/\kappa$ is already close to the correlation time of the field, which explains the tendency of the output field to approach a Poissonian statistics.

Another fundamental quantity to characterize the external field is the second-order intensity correlation function $g^{(2)}(t,t+\tau)$. It corresponds to the joint probability for recording photoelectric counts in the intervals $[t,t+\Delta t)$ and $[t+\tau,t+\tau+\Delta t)$, normalized by the probability for two independent photoelectric measurements. More precisely, let us consider the multicoincidence rates $w_m(t_1,t_2,\ldots,t_m)$, where $w_m(t_1,t_2,\ldots,t_m)\Delta t_1\Delta t_2\cdots\Delta t_m$ is the probability that one photoelectric count is recorded in each of the nonoverlapping intervals $(t_1<t_2<\cdots<t_m)$:

$$[t_1,t_1+\Delta t_1),[t_2,t_2+\Delta t_2),\ldots,[t_m,t_m+\Delta t_m).$$

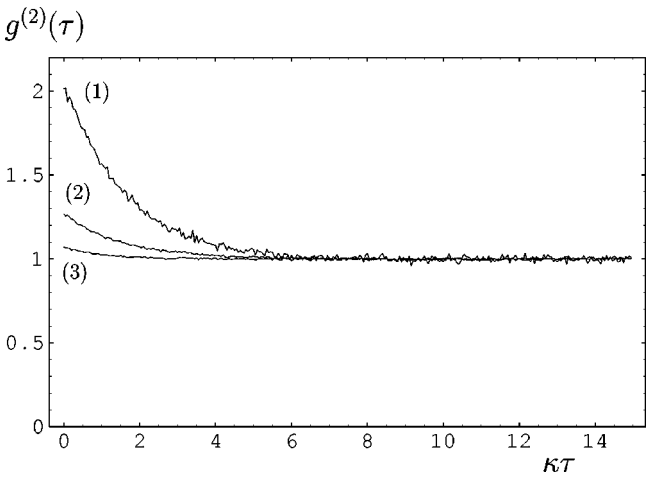

FIG. 6. Second-order intensity correlation for different values of the parameter $\Omega_1=g$: 40 MHz (1), 50 MHz (2), and 60 MHz (3). The ensemble average is performed over 5000 trajectories.

No restriction is placed on the number of counts recorded outside these intervals. The normalized second-order correlation function is defined in terms of these multicoincidence rates as [25]

$$g^{(2)}(t,t+\tau)=\frac{w_2(t,t+\tau)}{w_1(t)w_1(t+\tau)}. \tag{41}$$

If the light source is in a stationary regime, $g^{(2)}(t,t+\tau)$ is independent of t, and we have

$$g^{(2)}(t,t+\tau)=g^{(2)}(\tau). \tag{42}$$

Photon bunching and antibunching are traditionally defined in term of this quantity. In the simulations, in order to obtain $g^{(2)}(\tau)$, we have considered for each trajectory only the photoemissions that have occurred at a time $t>10/\kappa$. According to Fig. 3, we are already in a stationary regime. If a click is recorded at time t, we look to see if another click has been recorded in the time interval $[t+\tau,t+\tau+\Delta t)$. No restriction is placed on the number of counts recorded in the interval $(t,t+\tau)$. In order to ensure that only one click is registered in the interval $[t+\tau,t+\tau+\Delta t)$, it is necessary for Δt to be small in comparison to the cavity decay time. We have chosen $\Delta t=0.05/\kappa$. The results for $g^{(2)}(\tau)$ obtained from the simulations, for different values of the Raman coupling constant, are shown in Fig. 6. Note that, as the photon-number distribution evolves from super-Poissonian to Poissonian (see Fig. 5), photon bunching is reduced, in agreement with our expectation.

V. NONCLASSICAL REGIME

In this section, we will show how it is possible to reach a lasing regime with a clear nonclassical behavior. In order to do so it is necessary to tackle in a more direct way the motion- and field-dependent Stark-shift term of Eq. (18). This can be done by appropriately choosing the adjustable frequency shift $\delta\omega_1$. As shown in Appendix A, it is possible to choose $\delta\omega_1$ so as to remove the constant Stark-shift term

$-\hbar(|\Omega_1|^2/\Delta)\hat{A}_{22}$ of Eq. (18). In this section, we will choose $\delta\omega_1$ so as to remove not only the constant Stark-shift term, but also set to zero the contribution from the motion- and field-dependent Stark-shift term for a chosen Raman transition $|1,k+1,m+1\rangle\leftrightarrow|2,k,m\rangle$, that is,

$$\delta\omega_1=\frac{|\Omega_1|^2}{\Delta}-\frac{|g|^2}{2\Delta}[1+\cos(2\varphi_C)L^{(0)}_{(k+1)}(\eta^2_{2C})e^{-\eta^2_{2C}/2}]\times(m+1). \tag{43}$$

The chosen transition will be tuned to resonance, while other transitions remain off-resonance. As is shown in Appendix B, when we choose this resonance condition the effective Hamiltonian becomes $\hat{H}'_{\rm eff}=\hat{H}^R_{\rm eff}+\hat{H}^{S'}_{\rm eff}$, where $\hat{H}^R_{\rm eff}$ is given by Eq. (19) and

$$\frac{\hat{H}^{S'}_{\rm eff}}{\hbar}=-\frac{|g|^2}{2\Delta}\{[1+\cos(2\varphi_C)\hat{f}_0(\hat{a}^\dagger\hat{a};\eta_{2C})]\hat{b}^\dagger\hat{b}-[1+\cos(2\varphi_C)L^{(0)}_{(k+1)}(\eta^2_{2C})e^{-\eta^2_{2C}/2}](m+1)\}\hat{A}_{11}. \tag{44}$$

To get insight into the state-selectivity of the present dynamics, let us consider the flip operator

$$\hat{A}^{m';m'+1}_{2,k';1,k'+1}=|2,k',m'\rangle\langle 1,k'+1,m'+1| \tag{45}$$

for an arbitrary Raman transition $|1,k'+1,m'+1\rangle\leftrightarrow|2,k',m'\rangle$. The commutator between $\hat{A}^{m';m'+1}_{2,k';1,k'+1}$ and the Stark-shift Hamiltonian $\hat{H}^{S'}_{\rm eff}$, see Eq. (44), gives

$$[\hat{A}^{m';m'+1}_{2,k';1,k'+1},\hat{H}^{S'}_{\rm eff}]=-\hbar\frac{|g|^2}{2\Delta}\hat{A}^{m';m'+1}_{2,k';1,k'+1}\times\{[1+\cos(2\varphi_C)L^{(0)}_{(k'+1)}(\eta^2_{2C})e^{-\eta^2_{2C}/2}]\times(m'+1)-[1+\cos(2\varphi_C)L^{(0)}_{(k+1)}\times(\eta^2_{2C})e^{-\eta^2_{2C}/2}](m+1)\}, \tag{46}$$

so that the evolution caused by the Stark shift alone is

$$\hat{A}^{m';m'+1}_{2,k';1,k'+1}(t)=\hat{A}^{m';m'+1}_{2,k';1,k'+1}e^{i\Delta\omega t}, \tag{47}$$

where

$$\Delta\omega=\frac{|g|^2}{2\Delta}\{[1+\cos(2\varphi_C)L^{(0)}_{(k'+1)}(\eta^2_{2C})e^{-\eta^2_{2C}/2}](m'+1)-[1+\cos(2\varphi_C)L^{(0)}_{(k+1)}(\eta^2_{2C})e^{-\eta^2_{2C}/2}](m+1)\} \tag{48}$$

is the frequency Stark shift for the $|1,k'+1,m'+1\rangle\leftrightarrow|2,k',m'\rangle$ transition. In the following we will choose $k=m=0$ in Eq. (43), which tunes the $|1,1,1\rangle\leftrightarrow|2,0,0\rangle$ transition on resonance. The reason to consider this case is because, due to the cooling mechanism, the transition $|1,1,1\rangle\leftrightarrow|2,0,0\rangle$ is the dominant one. Moreover, no more than a single cavity photon exists for the states corresponding to this resonance condition. In this regime, one should expect the laser system to emit antibunched photons. Having set this chosen transition on resonance, let us see how big the frequency shift is for the neighboring transition $|1,2,2\rangle\leftrightarrow|2,1,1\rangle$. This frequency shift is obtained by setting $k'=m'=1$ in Eq. (48),

$$\Delta\omega=\frac{|g|^2}{2\Delta}\{2[1+\cos(2\varphi_C)L^{(0)}_2(\eta_{2C})e^{-\eta^2_{2C}/2}]-[1+\cos(2\varphi_C)L^{(0)}_1(\eta^2_{2C})e^{-\eta^2_{2C}/2}]\}. \tag{49}$$

Substituting in this equation the expressions for the Laguerre polynomials, we obtain

$$\Delta\omega=\frac{|g|^2}{2\Delta}[1+\cos(2\varphi_C)(1-3\eta^2_{2C}+\eta^4_{2C})e^{-\eta^2_{2C}/2}]. \tag{50}$$

In our scheme we use $\eta_{2C}=0.2$, so that $\eta^2_{2C}\ll 1$. This gives

$$\Delta\omega\simeq\frac{|g|^2}{2\Delta}[1+\cos(2\varphi_C)]. \tag{51}$$

For $\varphi_C=0$, which corresponds to setting the position of the center of the trap on an antinode of the standing wave of the cavity field, the value $\Delta\omega=|g|^2/\Delta$ attains its maximum.

To get some idea about the values of the parameters, we consider the situation for $g=60.0$ MHz, $\Delta=600.0$ MHz, and $\nu=100$ MHz. In this case, the maximum separation ($\varphi_C=0$) of the neighboring state relative to the chosen state of interest is $\Delta\omega=6.0$ MHz. The minimum separation ($\varphi_C=\pi/2$) is $\Delta\omega\simeq 3|g|^2\eta^2_{2C}/(2\Delta)=0.36$ MHz. In this case, the transition $|1,2,2\rangle\leftrightarrow|2,1,1\rangle$ is quite close to resonance.

Having chosen in Eq. (44) the resonance condition for the transition $|1,1,1\rangle\leftrightarrow|2,0,0\rangle$, we have seen from Eq. (51) how the frequency shift $\Delta\omega$ for the $|2,1,1\rangle\leftrightarrow|1,2,2\rangle$ transition can be changed by varying the position of the center of the trap with respect to the standing-wave cavity field. The dependence of this frequency shift on the phase φ_C results in a selective transition for the case $\varphi_C=0$, and basically no selective transition for the case $\varphi_C=\pi/2$. This selectivity has an evident impact on the cavity-field properties. In Fig. 7, we see how, changing only the phase of the cavity field, we observe a significant change of the average number of photons inside the cavity. Figure 8 displays, on the other hand, how the strongly selective tuning ($\varphi_C=0$) yields a clear nonclassical regime, with sub-Poissonian statistics in the number probability distribution of the intracavity field. Moreover, sub-Poissonian statistics and antibunching occur in the external field, as shown in Fig. 9 and Fig. 10, respectively. These results show how, by appropriately handling the motion- and field-dependent Stark shift, one has the possibility to significantly influence, through the choice of the phase of the cavity field, the properties of the intracavity and the emitted field.

Let us again compare the statistics of the intracavity field (Fig. 8) with that of the external field (Fig. 9). As already discussed in the previous section, the integration over a finite

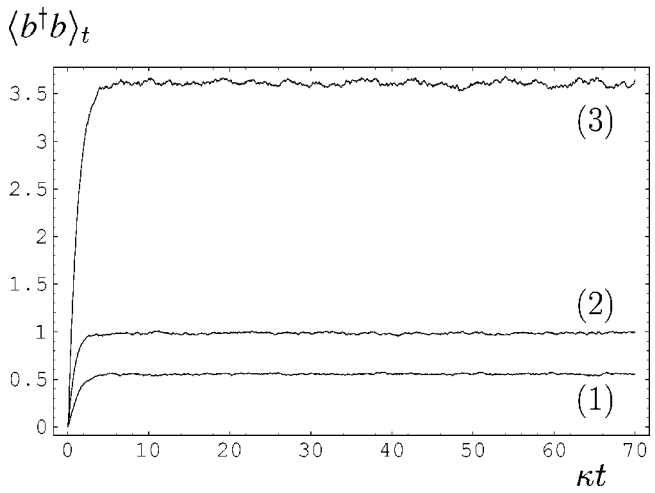

FIG. 7. Average number of photons inside the cavity. The value for $\Omega_1 = g$ is 60 MHz. The figures are for different values of the parameter φ_C: 0 (1), $\pi/4$ (2), and $\pi/2$ (3). The ensemble average is performed over 5000 trajectories.

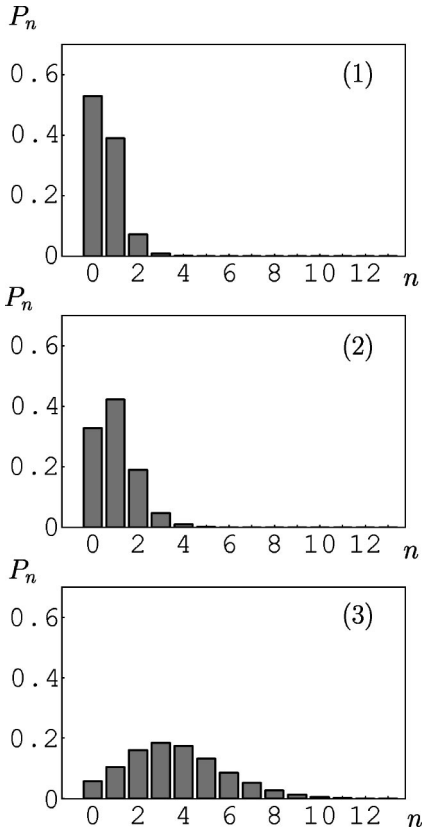

FIG. 8. Photon-number probability distribution for the photons inside the cavity at the time $t = 70/\kappa$. The value for $\Omega_1 = g$ is 60 MHz. The figures are for different values of the parameter φ_C: 0 (1), $\pi/4$ (2), $\pi/2$ (3). The values for $\overline{(\Delta n)^2}/\overline{n}$ are 0.80 (1), 0.84 (2), and 1.28 (3). The ensemble average is performed over 5000 trajectories.

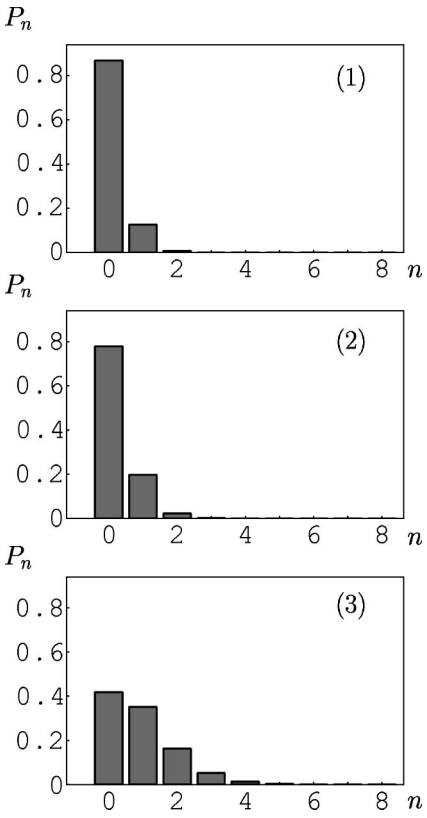

FIG. 9. Photon-number probability distribution for the photons detected outside the cavity for an integration time $T = 0.25/\kappa$. The value for $\Omega_1 = g$ is 60 MHz. The figures are for different values of the parameter φ_C: 0 (1), $\pi/4$ (2), $\pi/2$ (3). The values for $\overline{(\Delta n)^2}/\overline{n}$ are 0.96 (1), 0.97 (2), and 1.06 (3). The ensemble average is performed over 5000 trajectories.

measurement interval of size T in the case of the external field leads to a photocounting statistics that is closer to a Poissonian one than that for the intracavity field. Consequently, for a sub (super) -Poissonian number statistics of the intracavity field, the noise in the output statistics is expected to be increased (decreased), in full agreement with the results of our simulations.

VI. SUMMARY AND CONCLUSIONS

We have presented a scheme for a single-trapped-ion vibronic Raman laser where both the laser mode and the center-of-mass motion of the ion are quantized. The quantization of the center-of-mass motion in our scheme is a prerequisite for obtaining the inversion that is necessary for the lasing phenomenon. The combination of resolved-sideband laser cooling with an incoherent pump (on the resolved electronic carrier) saturating the vibronic transitions allows one to realize population inversions on the first vibronic sidebands. These inversions are used for lasing in a Raman scheme, in which a classical field is combined with a quantized cavity field mode to realize the coupling between the vibronic transitions and the cavity field. Moreover, the model accounts for cavity losses and the spontaneous electronic transitions of the ion that are needed for sideband cooling.

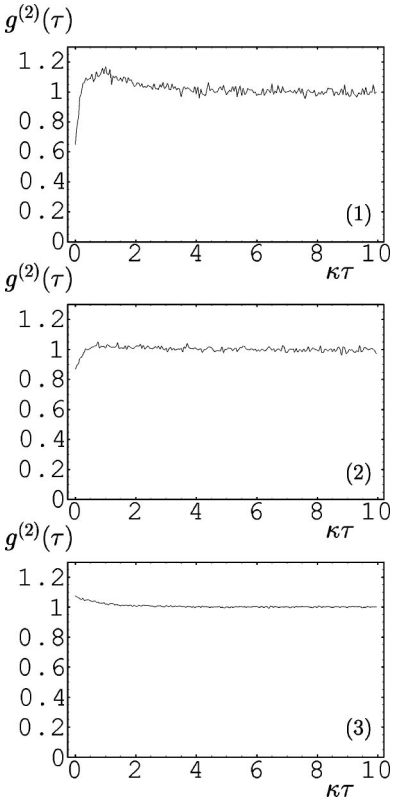

FIG. 10. Second-order intensity correlation. The value for $\Omega_1 = g$ is 60 MHz. The figures are for different values of the parameter φ_C: 0 (1), $\pi/4$ (2), and $\pi/2$ (3). The ensemble average is performed over 5000 trajectories.

We also take into consideration the nonlinearities that in general occur in the light-field assisted vibronic interaction of the trapped ion. In particular, we analyze the role played by nonlinear Stark shifts depending on the quantum states of the electron, the quantized motion of the ion, and the cavity field.

After deriving the basic master equation for the laser model, quantum-trajectory methods have been used for its solution. When the Stark-shift effects are minimized, a transition of the system from a super-Poissonian and photon-bunched light source to a Poissonian lasing regime is observed as the strength of the Raman coupling is increased. Such a transition to a lasing regime occurs already when the mean number of cavity photons is as small as about three.

When the nonlinear Stark shift is appropriately adjusted by changing the trap position, one can apply this effect to realize the laser action on a preferential vibronic transition, the other vibronic transitions being off-resonant. For example, one may support the laser action in such a manner that it is most probable to have zero or one photon inside the cavity. In such a case the intracavity field becomes sub-Poissonian. Consequently, also the output field is sub-Poissonian and displays photon antibunching.

ACKNOWLEDGMENTS

This work was supported by Deutscher Akademischer Austauschdienst (DAAD), Deutsche Forschungsgemeinschaft (DFG), Coordenação de Aperfeiçoamento de Pessoal de Ensino Superior (CAPES), Conselho Nacional de Desenvolvimento Científico e Tecnológico (CNPq), Fundação de Amparo à Pesquisa do Estado do Rio de Janeiro (FAPERJ), Fundação Universitária José Bonifácio (FUJB), and Programa de Apoio a Núcleos de Excelência (PRONEX).

APPENDIX A

The approximate non-Hermitian Hamiltonian, Eq. (8), and the relative effective Hamiltonian, Eq. (10), have been obtained using the following considerations [15]. When we have a term as $k\hat{x}(t)$ we write it as

$$k\hat{x}(t) = \eta(\hat{a}^\dagger e^{i\nu t} + \hat{a}e^{-i\nu t}), \tag{A1}$$

where η is the Lamb-Dicke parameter related to k. Then we use the Baker-Campbell-Hausdorff formula

$$\begin{aligned}\exp(i\eta\hat{a}^\dagger e^{i\nu t} + i\eta\hat{a}e^{-i\nu t}) &= \exp(i\eta\hat{a}^\dagger e^{i\nu t})\exp(i\eta\hat{a}e^{-i\nu t}) \\ &\times \exp\left(-\frac{\eta^2}{2}[\hat{a},\hat{a}^\dagger]\right).\end{aligned} \tag{A2}$$

Using Eqs. (A1) and (A2) we can obtain, neglecting terms oscillating with the vibrational frequency ν, the following formula:

$$\exp(ik\hat{x}(t) - m\nu t) \to \begin{cases} (i\eta\hat{a}^\dagger)^m \hat{f}_m(\hat{a}^\dagger\hat{a};\eta), & m \geqslant 0 \\ \hat{f}_{|m|}(\hat{a}^\dagger\hat{a};\eta)(i\eta\hat{a})^{|m|}, & m < 0, \end{cases} \tag{A3}$$

where $\hat{f}_m(\hat{a}^\dagger\hat{a};\eta)$ is defined in Eq. (9). Using this result it is easy to see that the two exponentials in Eq. (5) related with the incoherent laser and the cooling laser can be written as

$$e^{ik_{\rm inc}\hat{x}(t)} \to \hat{f}_0(\hat{a}^\dagger\hat{a};\eta_{\rm inc}), \tag{A4}$$

$$e^{i[k_2\hat{x}(t)+\nu t]} \to \hat{f}_1(\hat{a}^\dagger\hat{a};\eta_2)(i\eta_2\hat{a}). \tag{A5}$$

Equations (A4) and (A5) are used in Eq. (5) to obtain Eq. (8). The terms related to the Raman coupling in Eq. (5), i.e., the terms with g and Ω_1, have to be treated together. They produce the effective Hamiltonian $\hat{H}_{\rm eff}$, see Eq. (10), with the expressions for $\hat{H}^R_{\rm eff}(t)$ and $\hat{H}^S_{\rm eff}(t)$ given, before neglecting oscillating terms, by Eq. (11) and Eq. (13), respectively. If we choose $\delta\omega_1 = 0$, see Eq. (11), and use Eq. (A3), it is easy to see that

$$\begin{aligned}&\cos(k_C\hat{x}(t)+\varphi_C)e^{i[k_1\hat{x}(t)-\nu t]} \\ &= \frac{1}{2}(e^{i[k_C\hat{x}(t)+\varphi_C]} + e^{-i[k_C\hat{x}(t)+\varphi_C]})e^{i[k_1\hat{x}(t)-\nu t]} \\ &\approx \frac{e^{i\varphi_C}}{2}(i\eta_+\hat{a}^\dagger)\hat{f}_1(\hat{a}^\dagger\hat{a};\eta_+) + \frac{e^{-i\varphi_C}}{2}(i\eta_-\hat{a}^\dagger)\hat{f}_1(\hat{a}^\dagger\hat{a};\eta_-),\end{aligned} \tag{A6}$$

where

$$(k_1+k_C)\hat{x}(t)=\eta_+(\hat{a}^\dagger e^{i\nu t}+\hat{a}e^{-i\nu t}), \tag{A7}$$

$$(k_1-k_C)\hat{x}(t)=\eta_-(\hat{a}^\dagger e^{i\nu t}+\hat{a}e^{-i\nu t}). \tag{A8}$$

Moreover, we can obtain in the same way

$$[\cos(k_C\hat{x}(t)+\varphi_C)]^2\approx\frac{1}{2}[1+\cos(2\varphi_C)\hat{f}_0(\hat{a}^\dagger\hat{a};\eta_{2C})], \tag{A9}$$

where

$$2k_C\hat{x}(t)=\eta_{2C}(\hat{a}^\dagger e^{i\nu t}+\hat{a}e^{-i\nu t}). \tag{A10}$$

Using Eq. (A9) the Stark-shift Hamiltonian $\hat{H}^S_{\rm eff}(t)$ given by Eq. (13) is transformed into Eq. (18). Moreover, using Eq. (A6), the Raman Hamiltonian $\hat{H}^R_{\rm eff}(t)$ given by Eq. (11) is transformed into Eq. (19), where we have neglected the term with η_- in Eq. (A6) because we assume that $|k_1-k_C|\ll k_1$.

Let us now consider the Stark-shift Hamiltonian $\hat{H}^S_{\rm eff}$ given by Eq. (18). It is often useful to neglect the constant Stark-shift term $-\hbar(|\Omega_1|^2/\Delta)\hat{A}_{22}$ in this equation. Formally, this is equivalent to choosing an appropriate frequency shift $\delta\omega_1$ for the first laser. Changing to an interaction picture with respect to $-\hbar(|\Omega_1|^2/\Delta)\hat{A}_{22}$ and choosing $\delta\omega_1=|\Omega_1|^2/\Delta$, we obtain for the effective Hamiltonian $\hat{H}_{\rm eff}$ defined in Eq. (10), the expression, before elimination of oscillating terms,

$$\frac{\hat{H}_{\rm eff}(t)}{\hbar}=[-\Omega_R\cos(k_C\hat{x}(t)+\varphi_C)e^{i[k_1\hat{x}(t)-\nu t]}\hat{b}^\dagger\hat{A}_{12}+\text{H.c.}] -\frac{|g|^2}{\Delta}[\cos(k_C\hat{x}(t)+\varphi_C)]^2\hat{b}^\dagger\hat{b}\hat{A}_{11}. \tag{A11}$$

Using the substitutions (A6) and (A9) we obtain the following expressions for $\hat{H}^R_{\rm eff}$ and $\hat{H}^S_{\rm eff}$:

$$\frac{\hat{H}^R_{\rm eff}}{\hbar}=-\frac{1}{2}\Omega_R e^{i\varphi_C}(i\eta_+\hat{a}^\dagger)\hat{f}_1(\hat{a}^\dagger\hat{a};\eta_+)\hat{b}^\dagger\hat{A}_{12}+\text{H.c.} \tag{A12}$$

and

$$\frac{\hat{H}^S_{\rm eff}}{\hbar}=-\frac{|g|^2}{2\Delta}[1+\cos(2\varphi_C)\hat{f}_0(\hat{a}^\dagger\hat{a};\eta_{2C})]\hat{b}^\dagger\hat{b}\hat{A}_{11}, \tag{A13}$$

as given by Eq. (19) and Eq. (20).

APPENDIX B

As we have seen in Appendix A, it is possible to choose $\delta\omega_1$ so as to remove the constant Stark-shift term $-\hbar(|\Omega_1|^2/\Delta)\hat{A}_{22}$ from Eq. (18). In this appendix, we will see how we can choose $\delta\omega_1$ so as to remove not only the constant Stark-shift term, but also set to zero the contribution from the photon- and motional-number-dependent Stark shift for a chosen $|1,k+1,m+1\rangle\leftrightarrow|2,k,m\rangle$ transition. Let us consider $\hat{H}_{\rm eff}$ as given by Eq. (10), together with Eq. (11) and Eq. (13). We now change to an interaction picture with respect to $\hat{H}'_0$ given by

$$\frac{\hat{H}'_0}{\hbar}=-\frac{|g|^2}{2\Delta}[1+\cos(2\varphi_C)L^{(0)}_{(k+1)}(\eta^2_{2C})e^{-\eta^2_{2C}/2}] \times(m+1)\hat{A}_{11}-\frac{|\Omega_1|^2}{\Delta}\hat{A}_{22}. \tag{B1}$$

From the Heisenberg equation of motion for a generic operator $\hat{F}^{\rm I}$ in the interaction picture

$$i\hbar\frac{d\hat{F}^{\rm I}}{dt}=i\hbar\frac{\partial\hat{F}^{\rm I}}{\partial t}+[\hat{F}^{\rm I},\hat{H}'_0], \tag{B2}$$

we obtain then

$$\hat{A}^{\rm I}_{12}(t)=\exp\left\{i\left[-\frac{|g|^2}{2\Delta}[1+\cos(2\varphi_C)L^{(0)}_{(k+1)}(\eta^2_{2C})e^{-\eta^2_{2C}/2}] \times(m+1)+\frac{|\Omega_1|^2}{\Delta}\right]t\right\}\hat{A}^{\rm I}_{12}, \tag{B3}$$

where in the following we will use $\hat{A}_{12}$ for $\hat{A}^{\rm I}_{12}$. If we choose for $\delta\omega_1$ the value given in Eq. (43), we obtain a new effective Hamiltonian $\hat{H}'_{\rm eff}(t)$ given by the following expression:

$$\frac{\hat{H}'_{\rm eff}(t)}{\hbar}=[-\Omega_R\cos(k_C\hat{x}(t)+\varphi_C)e^{i[k_L\hat{x}(t)-\nu t]}\hat{b}^\dagger\hat{A}_{12}+\text{H.c.}] -|g|^2\Delta\left\{[\cos(k_C\hat{x}(t)+\varphi_C)]^2\hat{b}^\dagger\hat{b} -\frac{1}{2}[1+\cos(2\varphi_C)L^{(0)}_{(k+1)}(\eta^2_{2C})e^{-\eta^2_{2C}/2}] \times(m+1)\right\}\hat{A}_{11}. \tag{B4}$$

At this point we neglect oscillating terms as done in Appendix A. This yields

$$\frac{\hat{H}'_{\rm eff}}{\hbar}=[-\tfrac{1}{2}\Omega_R e^{i\varphi_C}(i\eta_+\hat{a}^\dagger)\hat{f}_1(\hat{a}^\dagger\hat{a};\eta_+)\hat{b}^\dagger\hat{A}_{12}+\text{H.c.}] -\frac{|g|^2}{2\Delta}\{[1+\cos(2\varphi_C)\hat{f}_0(\hat{a}^\dagger\hat{a};\eta_{2C})]\hat{b}^\dagger\hat{b} -[1+\cos(2\varphi_C)L^{(0)}_{(k+1)}(\eta^2_{2C})e^{-\eta^2_{2C}/2}](m+1)\}\hat{A}_{11}, \tag{B5}$$

as given for $\hat{H}'_{\rm eff}=\hat{H}^R_{\rm eff}+\hat{H}^{S'}_{\rm eff}$ by Eq. (19) and Eq. (44).

[1] Y. Mu and C. M. Savage, Phys. Rev. A **46**, 5944 (1992).
[2] C. Ginzel, H.-J. Briegel, U. Martini, B.-G. Englert, and A. Schenzle, Phys. Rev. A **48**, 732 (1993).
[3] M. Löffler, G. M. Meyer, and H. Walther, Phys. Rev. A **55**, 3923 (1997).
[4] T. Pellizzari and H. Ritsch, J. Mod. Opt. **41**, 609 (1994).
[5] D. Meschede, H. Walther, and G. Müller, Phys. Rev. Lett. **54**, 551 (1985); G. Rempe, N. Klein, and H. Walther, *ibid.* **58**, 353 (1987); G. Rempe, F. Schmidt-Kaler, and H. Walther, *ibid.* **64**, 2783 (1990).
[6] M. Brune, J. M. Raimond, P. Goy, L. Davidovich, and S. Haroche, Phys. Rev. Lett. **59**, 1899 (1987).
[7] K. An, J. J. Childs, R. R. Dasari, and M. S. Feld, Phys. Rev. Lett. **73**, 3375 (1994).
[8] P. Münstermann, T. Fischer, P. Maunz, P. W. H. Pinkse, and G. Rempe, Phys. Rev. Lett. **82**, 3791 (1999); P. Münstermann, T. Fischer, P. W. H. Pinkse, and G. Rempe, Opt. Commun. **159**, 63 (1999).
[9] J. Ye, D. W. Vernooy, and H. J. Kimble, Phys. Rev. Lett. **83**, 4987 (1999).
[10] P. W. H. Pinkse, T. Fischer, P. Maunz, and G. Rempe, Nature (London) **404**, 365 (2000).
[11] G. M. Meyer, M. Löffler, and H. Walther, Phys. Rev. A **56**, R1099 (1997).
[12] G. M. Meyer, H.-J. Briegel, and H. Walther, Europhys. Lett. **37**, 317 (1997).
[13] M. Löffler, G. M. Meyer, and H. Walther, Europhys. Lett. **40**, 263 (1997).
[14] G. Yu. Kryuchkyan and B. Kneer, Phys. Rev. A **60**, 5019 (1999).
[15] W. Vogel and R. L. de Matos Filho, Phys. Rev. A **52**, 4214 (1995).
[16] S. Wallentowitz and W. Vogel, Phys. Rev. A **55**, 4438 (1997).
[17] D. M. Meekhof, C. Monroe, B. E. King, W. M. Itano, and D. J. Wineland, Phys. Rev. Lett. **76**, 1796 (1996).
[18] C. Monroe, D. M. Meekhof, B. E. King, and D. J. Wineland, Science **272**, 1131 (1996).
[19] J. Dalibard and C. Cohen-Tannoudji, J. Opt. Soc. Am. B **6**, 2023 (1989).
[20] G. C. Hegerfeldt and T. S. Wilser, in *Proceedings of the Second International Wigner Symposium, 1991*, edited by H. D. Doebner, W. Sherer, and F. Schroeck (World Scientific, Singapore, 1992), p. 104; C. W. Gardiner, A. S. Parkins, and P. Zoller, Phys. Rev. A **46**, 4363 (1992); J. Dalibard, Y. Castin, and K. Mølmer, Phys. Rev. Lett. **68**, 580 (1992).
[21] R. Dum, H. Ritsch, and P. Zoller, Phys. Rev. A **45**, 4879 (1992).
[22] H. J. Carmichael, *An Open Systems Approach to Quantum Optics*, Lecture Notes in Physics Vol. m18 (Springer, Berlin, 1993).
[23] K. Mølmer, Y. Castin, and J. Dalibard, J. Opt. Soc. Am. B **10**, 524 (1993); B. M. Garraway and P. L. Knight, Phys. Rev. A **50**, 2548 (1994); M. B. Plenio and P. L. Knight, Rev. Mod. Phys. **70**, 101 (1998).
[24] Y. Castin and K. Mølmer, Phys. Rev. A **54**, 5275 (1996).
[25] W. Vogel, D.-G. Welsch, and S. Wallentowitz, *Quantum Optics. An Introduction* (Wiley-VCH, Berlin, 2001).